2. *Agrostat-PC: Production* (Computerized Information Series, Food and Agriculture Organization, United Nations, Rome, 1991).
3. *1990 Energy Statistics Yearbook* (Bureau of Statistics, United Nations, New York, 1992).
4. *Foreign Trade by Commodities* (Statistics Directorate, Organization for Economic Cooperation and Development, Paris, 1993).
5. Other studies have found significant reductions in crop yields in the United States and in the Kanto district of Japan as a result of O_3 pollution (*6, 7*).
6. R. M. Adams, J. D. Glyer, S. L. Johnson, B. A. McCarl, *J. Air Waste Manag.* **39**, 960 (1989).
7. K. Kobayashi, in *Tropospheric Ozone and the Environment II*, R. L. Bergland, Ed. (Air and Waste Management Association, Pittsburgh, 1992), pp. 537–551.
8. A. J. Haagen-Smit, *Ind. Eng. Chem.* **44**, 1362 (1952); J. H. Seinfeld *et al.*, *Rethinking the Ozone Pollution Problem in Urban and Regional Ozone Pollution* (National Academy Press, Washington, DC, 1991).
9. W. W. Heck, J. A. Dunning, I. J. Hindawi, *Science* **151**, 577 (1966).
10. V. C. Runeckles and B. I. Chevone, in *Surface-Level Ozone Exposures and Their Effects on Vegetation*. A. S. LeFohn. Ed. (Lewis, Chelsea, MI, 1992), pp. 189–270.
11. D. T. Tingey, W. E. Hogsett, E. H. Lee, in *Tropospheric Ozone and the Environment*, R. L. Bergland, D. Lawson, D. McKee, Eds. (Air and Waste Management Association, Pittsburgh, 1989), pp. 272–288.
12. C. A. Ennis, J. Smith, A. L. Lazrus, *Tellus* **45B**, 40 (1993).
13. F. M. Vukovich, W. D. Bach, B. W. Crissman, W. J. King, *Atmos. Environ.* **11**, 967 (1977); R. Guicherit and H. Van Dop, *ibid.*, p. 145; J. A. Logan, *J. Geophys. Res.* **94**, 8511 (1989); J. Fishman, F. M. Vukovich, D. R. Cahoon, M. C. Shipham, *J. Clim. Appl. Meteorol.* **26**. 1638 (1987).
14. NO_y denotes total reactive N and is equal to NO_x plus the N-containing products derived from the oxidation of NO_x.
15. The GFDL GCTM calculates time-dependent distributions of NO_y, NO_x, HNO_3, and peroxyacetylnitrate with a simplified photochemical scheme and 12 months of 6-hour wind, temperature, and precipitation fields from a parent global circulation model (*16, 17*). The model has 11 layers in the vertical direction and a horizontal resolution of ~265 km. Table 1 lists the NO_x sources included in our application of the model: the resulting [NO_y − NO_x] values generally agree to within 1σ SD of daytime averaged observations at a number of continental and remote locations (*18–21*).
16. P. S. Kasibhatla, H. Levy II, W. J. Moxim, *J. Geophys. Res.* **98**, 7165 (1993).
17. H. Levy II, W. B. Moxim, P. S. Kasibhatla, in *The Tropospheric Chemistry of O_3 in Polar Regions*, H. Niki and K. H. Becker, Eds. (NATO Advanced Study Institute Series, Springer-Verlag, Berlin, 1993), vol. I7, pp. 77–88.
18. D. D. Parrish *et al.*, *J. Geophys. Res.* **98**, 2927 (1993).
19. T. Wang, thesis, Georgia Institute of Technology, Atlanta (1992).
20. S. T. Sandholm *et al.*, *J. Geophys. Res.* **97**, 16481 (1992); E. L. Atlas *et al.*, *ibid.*, p. 10449.
21. A. Volz-Thomas *et al.*, in *Proceedings of EUROTRAC Symposium '92*, P. M. Borrell, Ed. (SPB Academic, The Hague, 1993).
22. W. L. Chameides *et al.*, *J. Geophys. Res.* **97**, 6037 (1992); S. Sillman, J. A. Logan, S. C. Wofsy, *ibid.* **95**, 5731 (1990).
23. M. Trainer *et al.*, *ibid.* **98**, 2917 (1993).
24. The growing season is defined as November through February for 90° to 23°S, all year for 23°S to 23°N, and May through August for 23° to 90°N.
25. Virtually identical exposure statistics were calculated with the distribution of all food crops summed together on the basis of their caloric content.
26. This estimate does not account for synergistic effects between O_3 and other pollutants, such as SO_2, or for the fertilizing effects of NO_x deposition. Although the synergistic effects of other pollutants may cause larger crop reductions than those estimated here (*12*), the latter effect is probably negligible. Application rates of N fertilizers to agricultural plots are generally more than 100 kg of N ha^{-1} $year^{-1}$ (*2*), whereas NO_x emissions from fossil fuel combustion and soil emissions in CSMAPs are 10 kg of N ha^{-1} $year^{-1}$ or less (Table 1).
27. P. Foster, *The World Food Problem* (Lynne Rienner, Boulder, CO, 1992); R. L. Naylor, *Provisioning the Cities into the 21st Century* (Institute for International Studies, Stanford University, Stanford, CA, 1993).
28. *Agricultural Statistics 1992* (U.S. Department of Agriculture, Government Printing Office, Washington, DC, 1992); *World Agricultural Production* (U.S. Department of Agriculture, Circular Series WAP 8-92, Washington, DC, 1992); additional statistics supplied by the Production Estimates and Crop Assessment Division of the U.S. Department of Agriculture, Washington, DC.
29. E. Mathews, *Atlas of Archived Vegetation, Land-Use and Seasonal Albedo Data Sets, NASA Tech. Memo 86199* (Goddard Space Flight Center, Institute for Space Studies, New York, 1985).
30. W. A. Kaplan, S. C. Wofsy, M. Keller, J. M. da Costa, *J. Geophys. Res.* **93**, 1389 (1988); P. S. Bakwin *et al.*, *ibid.* **95**, 16755 (1990).
31. E. J. Williams, A. Guenther, F. C. Fehsenfeld, *ibid.* **97**, 7511 (1992); M. F. Shepard, S. Barzetti, D. R. Hastie, *Atmos. Environ.* **25A**, 1961 (1991).
32. Cereal crops are the total of the production of wheat, rice, and coarse grains such as maize, millet, oats, rye, and barley.
33. Cereal production was derived from country-by-country statistics for 1991 (*2*), except for the United States, Canada, China, and the former Soviet Union, where 1991 statistics at the state or province level were used (*28*). These production statistics were geographically disaggregated onto a 1° by 1° grid with the land use data of Mathews (*29*) renormalized so that the total cultivated area within a given country did not exceed the value reported by the Food and Agriculture Organization (*2*).
34. The NO_x soil source was estimated for 10 generic biomes (water, ice, desert, tundra, scrubland, grassland, woodland, forest, rainforest, and agricultural lands) and geographically distributed with renormalized land use data (*29*). Emissions are assumed to be 0 for water, ice, desert, and scrubland and 3 and 0.5 ng of N per square meter per second for rainforests in the dry and wet seasons, respectively (*30*). Emissions for all other biomes are given by $A \cdot \exp(0.071T)$, where T is temperature (in degrees Celsius) and A (nanograms of N per square meter per second) is a fitting parameter for each biome (*31*). For agricultural lands, A is $0.28(F)$ during the growing season (where F is the fertilization rate in kilograms of N per hectare per month) (*31*) and is equal to that for grasslands during the nongrowing season. The fertilizer-induced soil source is the flux obtained with N fertilization rates reported by the Food and Agriculture Organization (*2*) minus the flux obtained assuming all agricultural lands emit in a manner similar to that of grasslands.
35. D. A. Lashof and D. A. Tirpak, *Policy Options for Stabilizing Global Climate* (Hemisphere, New York, 1990).
36. H. Levy II, W. J. Moxim, P. S. Kasibhatla, J. A. Logan, in *Global Biomass Burning: Atmospheric, Climatic, and Biospheric Implications*, J. S. Levine, Ed. (MIT Press, Cambridge, MA, 1991), pp. 363–369.
37. P. S. Kasibhatla, *Geophys. Res. Lett.* **98**, 1707 (1993).
38. ——, H. Levy II, W. J. Moxim, W. L. Chameides, *J. Geophys. Res.* **96**, 18631 (1991).
39. This research was supported in part by the NSF under grant ATM-9213643 and by the National Oceanic and Atmospheric Administration under grant NA36GP0250. We thank R. Naylor and J. A. Logan for their helpful comments and suggestions, E. Mathews for supplying the global land use data set, and T. Rocke for supplying crop statistics.

4 November 1993; accepted 15 February 1994

Unexpected Square Symmetry Seen by Atomic Force Microscopy in Bilayer Films of Disk-Like Molecules

Nicholas C. Maliszewskyj, Paul A. Heiney,* Jack Y. Josefowicz, John P. McCauley Jr.,† Amos B. Smith III

Thin films of disk-shaped molecules are expected to display anisotropic optical and transport properties, leading to applications in optical display or sensor technologies. Bilayer Langmuir-Blodgett films of monomeric triphenylene mesogens have been studied by atomic force microscopy. The triphenylene cores of the constituent molecules tend to promote the formation of columnar structures in the plane of the substrate and along the direction of deposition of the film. Atomic force microscopy images of bilayer Langmuir-Blodgett films revealed two types of structure, one corresponding to an aligned columnar structure and the other to an unusual square lattice, which may result from the superposition of columnar structures in adjacent layers that intersect at near right angles. Annealing such bilayers near the melting point of the bulk compound improved the structural ordering by reducing the angular spread of orientations associated with the well-developed columnar structure in some areas and by producing a more distinct square lattice in other areas of the sample.

Langmuir-Blodgett (LB) films (*1, 2*) have long been of interest both as model systems for two-dimensional (2D) physics and for their promise in technological applications. Although most research in this area has concentrated on LB films of amphiphilic rod-like molecules, disk-shaped mesogens exhibiting columnar liquid crystalline phases (*3*) have been shown to form Langmuir (*4*) and LB films (*5, 6*). The electronic conductivity of doped bulk discotic mesophases is highly anisotropic, with most of the conduction occurring along the column axis (*7*). This suggests that thin films composed of disk-shaped molecules might also be expected to display anisotropic transport properties; such anisotropic films could potentially be used for optical displays and other electronic devices such as pressure sensors (*8*).

Surface pressure versus molecular area (Π-A) measurements of Langmuir films of discogenic molecules (*4, 6*) indicate that discotic mesogens can adopt two possible types of packing at the air-water interface. Large, flexible cores with long substituents and highly polar anchor groups can drive molecules to sit with the cores parallel ("face-on") to the interface. Alternatively, strong π-π interactions of the cores may lead to cofacial packing with the planes of the cores perpendicular ("edge-on") to the interface. It is reasonable to anticipate that the structure of the molecular film after being transferred to a solid substrate will be similar to that at the air-water interface, although this is by no means assured.

To make meaningful progress in the development of uses for films of these unusual mesogens, it is necessary to understand the microstructures present in these films and to correlate them with the technologically useful macroscopic anisotropic properties. There have been a number of studies of the macroscopic anisotropies manifested in multilayer films of polymeric (*6*) and monomeric (*9–11*) discogenic compounds, but attempts to ascertain the microscopic structure on the basis of these observations have been primarily conjectural. Atomic force microscopy (AFM) (*12*) is a useful probe of microscopic structures, including those formed on nonconductive surfaces (*13*), down to angstrom resolution. AFM is especially well suited to surfaces that are extremely flat, such as LB films (*14, 15*), as well as to transferred, freely suspended liquid crystal films (*16*). AFM has also been used to image drop-coated films with some surface modification (*17*).

We recently (*4*) reported the synthesis and characterization by Π-A isotherms of the triphenylene monomer 6,7,10,11-tetrakis(pentyloxy)-2,3-triphenylenedicarboxylic acid dibutyl ester (**1**), followed by AFM and x-ray diffraction (XRD) measurements of the same compound (*5*).

1

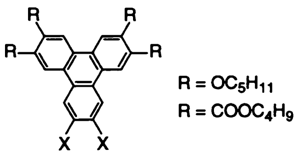

Bulk samples of **1** display a D_{hd} ("disordered hexagonal discotic") columnar liquid crystal mesophase at room temperature with an intercolumnar spacing of 20 Å and have a phase transition to an isotropic liquid at 167°C. In the D_{hd} phase, molecules are arranged in hexagonal arrays of columns. Π-A isotherms indicate that

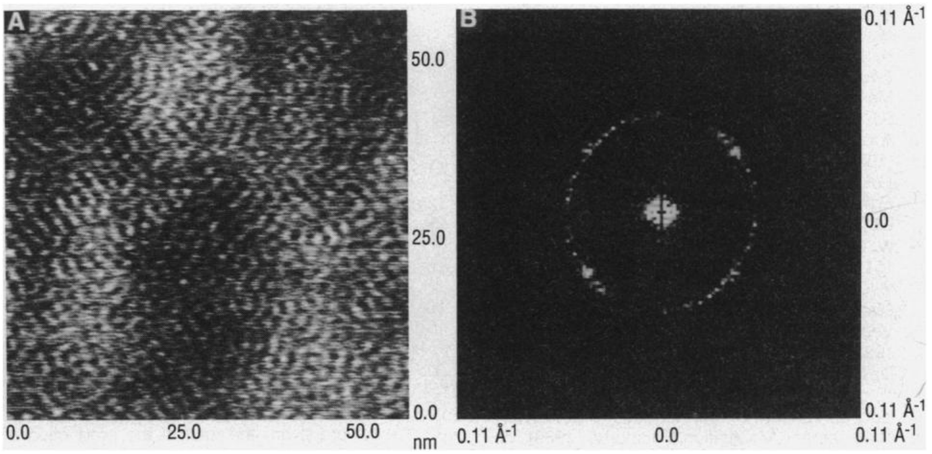

Fig. 1. (**A**) Typical AFM image of a LB bilayer of **1** on alkylated Si. (**B**) FT of unheated bilayer image, showing a ring corresponding to the 18 Å intercolumnar spacing, with a weak fourfold modulation.

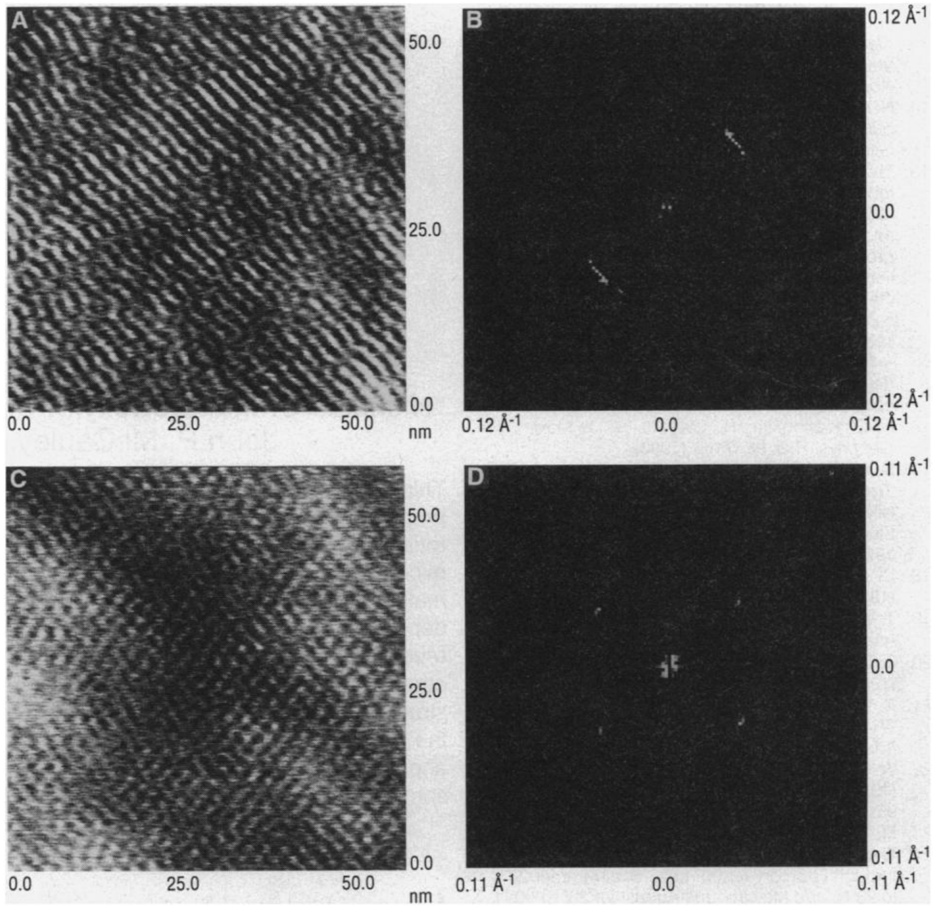

Fig. 2. On heating a bilayer film of **1** near the clearing point, two types of morphologies resolve themselves. (**A**) The columnar structure seen in the monolayer may become more distinct, although it is still possible to distinguish mismatches between layers. (**B**) FT of (A). Arcs similar to those seen in the monolayer are observed, with a somewhat larger azimuthal range. (**C**) Alternatively, a structure with approximately square symmetry may appear. (**D**) FT of (C). The fourfold modulation in the ring of correlations seen in the FT of Fig. 1 has sharpened up into spots with a roughly 90° angular separation.

N. C. Maliszewskyj and P. A. Heiney, Department of Physics and Laboratory for Research on the Structure of Matter, University of Pennsylvania, Philadelphia, PA 19104, USA.

J. Y. Josefowicz, Department of Materials Science and Engineering, University of Pennsylvania, Philadelphia, PA 19104, and Hughes Research Laboratories, Malibu, CA 90265, USA.

J. P. McCauley Jr. and A. B. Smith III, Chemistry Department and Laboratory for Research on the Structure of Matter, University of Pennsylvania, Philadelphia, PA 19104, USA.

---

*To whom correspondence should be addressed.

†Present address: Neose Pharmaceuticals, Inc., 102 Witmer Road, Horsham, PA 19104–2279, USA.

these molecules adopt an edge-on packing at the air-water interface. Our AFM measurements (5) indicated that in monolayer films of this compound the edge-on structure at the interface is transferred to a solid substrate, and that the molecules in the LB film are organized in columns with an intercolumnar spacing of ~18 Å and a spread in orientations of ~35° about the direction of deposition of the film. Thus, the molecules are arranged into columns in the bulk, at the air-water interface (at least as inferred from molecular areas), and in monolayer films on the solid substrate. XRD studies of multilayer films reveal that the material forms bulk droplets of liquid crystal instead of lamellae, but for a small number of layers we believe that the film is essentially lamellar. Here we present measurements of bilayer films of **1**, showing that in many cases the second layer is not formed with its columns parallel to those of the first, as one would expect, but perpendicular. Furthermore, this unusual behavior persists after thermal annealing of the samples.

Langmuir and LB films of **1** were prepared as previously described (*4, 5, 18*). To form bilayer films, we dipped and then withdrew the substrate through the surface film without intervening cleaning of the surface. AFM images were obtained with a Nanoscope III AFM (*19*) at 21°C, as previously described (*5, 20*). A typical AFM image of an as-prepared LB bilayer of **1** is shown in Fig. 1A. Some regions are characterized by the columnar ordering seen in monolayer films (5), as one might expect, but many regions exhibit an unusual structure with approximately square symmetry. The spacing between maxima is about 18 Å, the typical intercolumnar distance seen in the monolayer. A typical Fourier transform (FT) for one of these images is shown in Fig. 1B. The intensity is confined in a ring whose radius corresponds to the inverse of the intercolumnar spacing. Four intensity maxima are evenly spaced around the ring. This image is consistent with that expected for a collection of square lattices with slightly different orientations.

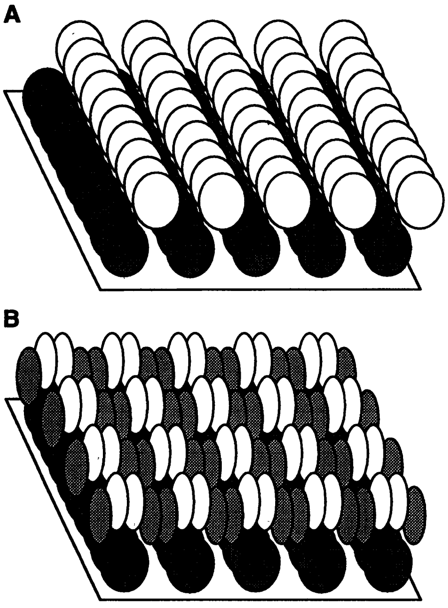

Fig. 3. Possible models for structures observed in bilayer LB films of **1**. (**A**) Parallel columnar structure. Columns in adjacent layers align in the same direction, as is seen in the bulk liquid crystalline phase. (**B**) Square lattice structure. Molecular directors in adjacent layers are rotated with respect to each other by ~90°, giving rise to a height modulation with apparent square lattice symmetry.

After heating (*18*) the substrate to 167°C for 6 to 12 hours and then cooling back to room temperature, two distinct morphologies are seen in AFM images (Fig. 2, A and C). In some cases, a columnar structure is observed, similar to that expected if the columns on the first and second layers became parallel (Fig. 2A); when extended to an infinite number of layers this would yield the known hexagonal bulk columnar structure. FTs of AFM images of these regions resemble FTs of the monolayer. In other regions, a more distinct square lattice is observed. The real space image is similar to that seen in the unheated film, but the order is even more distinctive (Fig. 2C), and the FT (Fig. 2D) of these regions shows a sharpening of the 2D lattice maxima into Bragg spots indicative of long-range order. Our models for these two structures are illustrated in Fig. 3. Although liquid crystalline materials can often be aligned by the application of magnetic fields, annealing a bilayer LB film of **1** at 165°C in a 3-kG field for ~48 hours resulted in no observable enhancement of the columnar structure.

The most likely explanation for the observation of a 2D lattice with approximately square symmetry is that the two layers each have columnar structure, but that the columns in the top layer are roughly perpendicular to those in the bottom layer; the heights of the molecules in the top layer are thus modulated by the periodicity of the lower layer. We have previously shown (5) that the columns in an LB monolayer of **1** lie predominantly along the dipping direction, but that there is a ~35° spread in the orientations. To form our bilayers, we dipped and then withdrew the substrate, so that the two deposition directions were parallel. We would then naturally expect that the columns in the two layers would be roughly parallel, but that there would be a wide distribution of relative orientations of columns in the first and second layers. The fact that, after annealing, we see two predominant morphologies indicates that there may be two minima in the orientational potential energy: one at 0°, analogous to the liquid crystalline D_{hd} phase (as shown in Fig. 3A), and another, perhaps broader one at ~90°, as is seen (Fig. 3B) in square lattice domains of the annealed films. Since the square structure has no analog in bulk samples of **1**, the evolution of this structure upon multilayer formation is an intriguing, unresolved issue.

REFERENCES AND NOTES

1. G. L. Gaines, *Insoluble Monolayers at Liquid Gas Interfaces*, (Interscience, Boston, 1966).
2. A. Ulman, *Introduction to Ultrathin Organic Films* (Academic Press, Boston, 1991).
3. S. Chandrasekhar and G. S. Raganath, *Rep. Prog. Phys.* **53**, 57 (1990).
4. N. C. Maliszewskyj, P. A. Heiney, J. K. Blasie, J. P. McCauley Jr., A. B. Smith III, *J. Phys. II (France)* **2**, 75 (1992).
5. J. Y. Josefowicz *et al.*, *Science* **260**, 323 (1993).
6. A. Albrecht, W. Cumming, W. Kreuder, A. Laschewskyj, H. Ringsdorf, *Colloid Polym. Sci.* **264**, 659 (1986); E. Orthmann and G. Wegner, *Angew. Chem.* **98**, 1114 (1986); O. Karthaus, H. Ringsdorf, V. V. Tsukruk, J. H. Wendorff, *Langmuir* **8**, 2279 (1992).
7. G. B. M. Vaughan, P. A. Heiney, J. P. McCauley Jr., A. B. Smith III, *Phys. Rev. B* **46**, 2787 (1992).
8. S. Jin, T. H. Tiefel, R. Wolfe, R. C. Sherwood, J. J. Mottine Jr., *Science* **255**, 446 (1992).
9. I. R. Peterson, *Thin Solid Films* **116**, 357 (1984).
10. P.-A. Albouy *et al.*, *Langmuir* **8**, 2262 (1992).
11. M. Vandevyver *et al.*, *ibid.* **9**, 1561 (1993).
12. G. Binnig, C. F. Quate, C. Gerber, *Phys. Rev. Lett.* **56**, 930 (1986).
13. T. R. Albrecht and C. F. Quate, *J. Appl. Phys.* **62**, 2599 (1988).
14. E. Meyer *et al.*, *Nature* **349**, 398 (1991).
15. D. K. Schwartz, R. Viswanathan, J. A. N. Zasadzinski, *Phys. Rev. Lett.* **70**, 1267 (1993).
16. R. M. Overney *et al.*, *Langmuir* **9**, 341 (1993).
17. V. V. Tsukruk, D. H. Reneker, H. Bengs, H. Ringsdorf, *ibid.*, p. 2141.
18. Substrates used for these studies were Si(100) silicon wafers coated with a self-assembled monolayer of hexadecyltrichlorosilane (*21*). All specimens were stored in argon after manufacture. Some samples were imaged immediately after fabrication. Others were annealed in an argon-filled oven, within which the temperature was maintained near the melting point of the bulk monomer, followed by slow cooling to room temperature.
19. Digital Instruments, Santa Barbara, CA.
20. Several different areas of any given film were imaged in order to obtain a more representative observation of the morphologies present in the film. Furthermore, the structures imaged were found to be stable over the course of several hours of scanning, to scale with scan size, and not to change when scanning angles were varied over a range of 0° to 90°. Between the two extreme angles the scanning tip is dragged parallel and perpendicular to the length of the cantilever. None of the images presented in this paper has been filtered, enhanced, or otherwise altered in any way.
21. J. Sagiv, *J. Am. Chem. Soc.* **102**, 92 (1980).
22. We thank G. C. Farrington, University of Pennsylvania, and R. A. Reynolds and A. N. Chester, Hughes Research Labs, Malibu, CA, for their support. We thank J. K. Blasie for the use of his Langmuir trough. Supported by National Science Foundation grants DMR MRL 92-20668 and DMR 89-01219.

5 November 1993; accepted 1 February 1994